



Optimization of mass flow rate ratio of water and air in humidification–dehumidification desalination systems

Kien Quoc Vo^a, Chi Hiep Le^{a,*}, An Quoc Hoang^b

^aDepartment of Heat and Refrigeration, Ho Chi Minh City University of Technology, VNU-HCM, 268 Ly Thuong Kiet Street, Ward 14, District 10, Ho Chi Minh City, Vietnam, emails: vkquoc@hcmut.edu.vn (K. Quoc Vo), lechihiep@hcmut.edu.vn (C. Hiep Le)

^bHo Chi Minh City University of Technology and Education, 01 Vo Van Ngan Street, Linh Chieu Ward, Thu Duc City, Ho Chi Minh City, Vietnam, email: hanquoc@hcmute.edu.vn

Received 10 July 2021; Accepted 4 December 2021

ABSTRACT

For the purpose of optimizing the mass flow rate ratio of water and air (m) working in a closed air open water humidification–dehumidification desalination (CAOW-HDD) system, many theoretical and experimental studies were done. The research results show that the average errors between the theoretical calculations and experimental data are less than 2.63%. Based on the theoretical analysis by applying Pinch technology, a related simulation program was built in order to investigate the effect of operating parameters such as the spraying water temperature (t_3), the feed water temperature (t_1) and the minimum temperature difference (ΔT_{\min}) on the heat recovery ratio (f), the gained output ratio (GOR) and the optimum value of m . It is confirmed that, GOR is a concave function of the temperature t_3 and it is maximized for values of ΔT_{\min} ranging from 2°C–5°C and for values of t_3 ranging from 60°C–74°C. It is also concluded that the lower the minimum temperature difference ΔT_{\min} and the lower the temperature t_3 , the higher the optimum GOR. In addition, the simulation results also show that the lower the ΔT_{\min} , the higher the GOR. At $\Delta T_{\min} = 2^\circ\text{C}$, the value of GOR reaches 2.86. Based on the regression analysis, the equation used to determine the optimum value of m was developed and it is concluded that m depends not only on the temperature t_3 with correlation coefficient $R^2 = 1$, but also on the temperature t_1 with correlation coefficient $R^2 = 0.998$.

Keywords: HD desalination; Closed air open water; Heat recovery; Pinch technology

1. Introduction

Scarcity of fresh water and climate change are two issues that are threatening human life. The world's population has grown rapidly, and the speed of urbanization and industrialization in many countries has made water sources more polluted and depleted [1,2]. Desalination of seawater to provide fresh water is one of the pioneering methods which have been used to produce clean water. Today, desalination of sea water is still one of the key methods in providing fresh water. To solve the problem of fresh water

shortages for urban areas, the most widely used desalination technologies are reverse osmosis (RO) and multi stage flash (MSF). For fresh water demand in the range of 5–100 m³/d production costs are immense when using RO or MSF technology [3–5]. Humidification–dehumidification desalination (HDD) technology is another method which is still being researched and developed. Further study is needed to increase the performance of the HDD system [6].

HDD has many advantages that traditional desalination methods cannot achieve, such as: easy fabrication, low investment cost, low operating cost, the ability to operate

* Corresponding author.

at low pressure and work with a low temperature heat source. HDD is the most feasible method to provide fresh water for small-scale decentralized units [7–9]. In addition, the HDD system has the ability to utilize the waste heat of condensation which in turn is used to heat the feed water. The more heat that is utilized, the higher the efficiency of the HDD system. This conclusion has been determined in many studies on the optimization of the HDD system to improve its performance.

The cycle of a CAOW-HDD system is shown in Fig. 1. The CAOW-HDD system has five devices: a humidifier, dehumidifier, heater, pump, and circulation fan. The humidifier includes packing bed materials and sprayers. The cooling water condenser is included inside the dehumidifier.

In CAOW-HDD, the values of relative humidity at points 5 and 6 in Fig. 1 are nearly 100% [7,8,10–12]. In the humidifier, hot water 3 after being heated in the heater is then pumped into the nozzles and sprayed onto the cooling pad materials. Cold air (point 5) is blown in the opposite direction to the hot water 3, it is then heated by hot water 3 and its humidity content gradually increases, at the exit of the humidifier it becomes nearly saturated air (point 6). Air at state 6 is then sent to the dehumidifier in which some heat is rejected to feed water 1 and a quantity of vapor water contained in saturated air 6 is condensed. At the exit of the dehumidifier, air 6 becomes cooler with a lower humidity content. The feed water 1 after being primarily heated in the dehumidifier (point 2) is then secondarily heated in the heater (point 3) and the excess spraying water is collected at the bottom of the humidifier (point 4).

Studies on energy, entropy and exergy analysis conducted by many researchers to enhance the efficiency of the HDD system have been done. Mistry [5] presented optimum operating parameters and configurations. Their results confirmed that the lower the minimum temperature difference (ΔT_{\min}), the higher the gained output ratio (GOR). In addition, the performance of cycles also depends on operating conditions. Hou et al. [7] conducted a study on optimizing the performance of a solar HDD system using Pinch analysis; their results confirmed that there is an optimum value of m corresponding to each temperature

couple of feed water and spraying water. The heat recovery rate (f) at the optimum value of mass flow rate ratio of water and air (m) corresponding to temperature of spraying water $t_3 = 80^\circ\text{C}$ and the temperature of feed water $t_1 = 30^\circ\text{C}$ is 0.67. When the t_3 is constant, the lower the t_1 , the lower the optimum value of m . At $\Delta T_{\min} = 1^\circ\text{C}$, the heat recovery rate ratio is 0.75. Narayan [13] conducted a thermal design of HDD, and from the results, it is clear that when the heat capacity rate ratio equals 1, the GOR is maximized. Sharqawy et al. [14] conducted an optimum thermal design of HDD systems with the results showing that the GOR is maximized at the optimum value of m . It is also clear that, the larger size of the humidifier and dehumidifier, the higher the GOR. Soufari et al. [15] presented the performance optimization of the HDD process using mathematical programming. From the results, it is clear that there is an optimum value of m which is the most influential parameter affecting the performance of the HDD process. In addition, according to [12], t_3 is also an important parameter and it is confirmed that the higher the t_3 , the higher the productivity and the lower the heat transfer area. At an optimum operating temperature, the supplying heat is minimized. Huang et al. [16] conducted an experimental study and optimized the energy consumption of the HDD system. Their results have concluded that the higher the required rate of evaporation, the higher the value of optimized specific total energy consumption. The mass flow rate of air should be as small as possible. At the inlet of the humidifier, it is a priority to adjust the mass flow rate and the temperature. The optimum specific total energy consumption is 822.676 kJ/kg. Huang et al. [17] presented the determination of optimum working parameters in a HDD system by a graphical method. Their results have concluded that in the case where ΔT_{\min} at the Pinch point of the humidifier equals 1, when the ΔT_{\min} at the Pinch point of the dehumidifier equals 1, the specific energy consumption is minimized and the GOR value can reach to 3.978 at the $t_3 = 65^\circ\text{C}$. Mohamed et al. [18] presented a theoretical and experimental study on a HDD system. Their results have concluded that there is an optimum value of m . The average productivity is 2.45 kg/h and the estimated cost per 1 L of fresh water is about 0.047 US\$. The effect of air and feed water flow rate on GOR and clean water yield was carried out in a subsequent study [19]. The results show that when increasing the air flow rate, the productivity is improved but the GOR decreases. In addition, when increasing the feed water flow rate, both productivity and GOR are improved. Alrbai et al. [20] analyzed the energy and exergy balances of the HDD system by fogging technology with two nozzle diameters (20 and 30 microns). Their results show that, at a mass flow rate ratio of 0.78, the maximum value of GOR and the minimum value of specific entropy production are 3.4 and 0.235 kJ/(kg K), respectively.

In our previous study [21], the optimized working parameters of the CAOW-HDD system using Pinch technology was performed. The study results show that, the optimum value of m depends on t_3 , t_1 and ΔT_{\min} .

The studies presented above prove that, there is obviously an optimum value of m for maximizing the performance of the HDD system. But these studies have

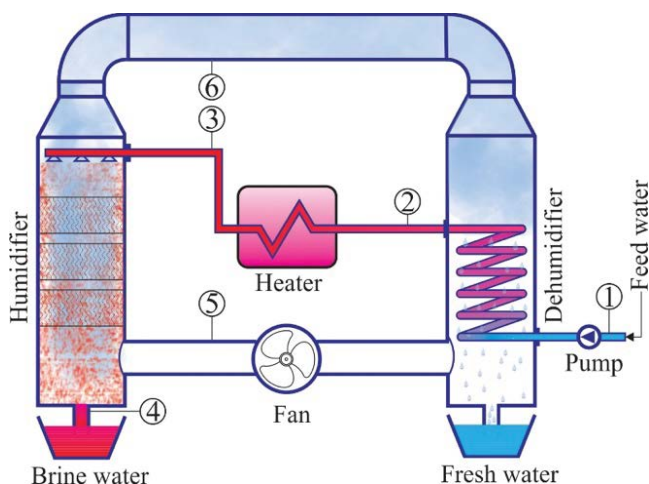


Fig. 1. CAOW-HDD system scheme.

not yet shown the method to determine this value. For the purpose of developing the equation to determine the optimum value of m based on the input parameters of CAOW-HDD and for the purpose of proposing a suitable spraying water temperature range for gaining the maximum value GOR, this paper presents the results done by Pinch technology and related experiments to study the effect of the operating parameters on the GOR.

2. Theoretical model

To optimize the performance of HDD system, Pinch technology [22] is one of the first choices of many researcher. In this study, Pinch technology is used to optimize the GOR of the CAOW-HDD. In our previous study [21], based on Pinch technology, we have achieved some initial results in optimizing the operating parameters of HDD systems.

To complete the optimization of the HDD system, in this study, Pinch technology continues to be used and verified by experimental results.

Based on the laws of Thermodynamic and Heat transfer, Fig. 2 describes the process of changing the state of working fluids in the CAOW-HDD system.

In the CAOW-HDD system, the air flow acts as cold stream in the humidifier, but in the dehumidifier it acts as hot stream. The hot stream in the humidifier is the spraying water and the cold stream in the dehumidifier is the feed water.

Based on the heat and mass transfers presented in Fig. 2, the relationship between the temperature and the enthalpy of the hot stream and the cold stream are shown in Fig. 3.

Fig. 3 shows that the recovered heat, waste heat and added heat are easily determined by Pinch analysis. Under the same t_3 and ΔT_{min} when the value of m is changed, the recovered heat, waste heat and added heat will also change. Based on these results, the optimum working parameters of the CAOW-HDD system can be determined.

The waste heat, the recovered heat and the added heat are presented below. Heat loss to the surroundings has been ignored.

$$Q_{wa} = Q_{add} = \dot{m}_w (h_3 - h_2) \tag{1}$$

$$Q_{rec} = \dot{m}_w (h_3 - h_4) = \dot{m}_w (h_2 - h_1) = \dot{m}_a (h_6 - h_5) \tag{2}$$

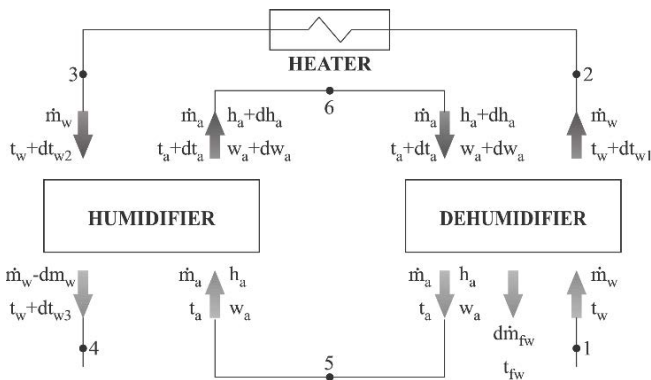


Fig. 2. Mathematical model in the CAOW-HDD system.

Fresh water is obtained by condensing water vapor in the air. In this process the humidity content of air is changed, so that the mass flow rate of fresh water is calculated as below:

$$\dot{m}_{fw} = \dot{m}_a (w_6 - w_5) \tag{3}$$

Heat recovery ratio:

$$f = \frac{Q_{rec}}{Q_{rec} + Q_{add}} \tag{4}$$

Gained output ratio:

$$GOR = \frac{\dot{m}_{fw} \cdot r}{Q_{add}} \tag{5}$$

Mass flow rate ratio of water and air:

$$m = \frac{\dot{m}_w}{\dot{m}_a} \tag{6}$$

Enthalpy of water:

$$h_w = C_{p_w} \cdot \dot{m}_w \cdot t \tag{7}$$

Enthalpy of saturated air [23]:

$$h_a = \exp(2.39329 + 0.10648t - 0.00135t^2 + 0.000010058t^3) \tag{8}$$

3. Experimental setup

The experimental model is shown in Fig. 4. The humidifier is made from 304 stainless steel with a square section. The dimensions of the humidifier are 220 cm height, 30 cm in length, and 30 cm in width. Five layers of cooling pad paper are arranged inside the humidifier with the distance two layers at 10 cm. The cross-sectional area of each layer is 30 cm × 30 cm and the height is 15 cm. Nine nozzles are arranged on the top of the humidifier at equal distances. A thin layer of cotton textile is glued inside the walls of the humidifier to reduce the speed of

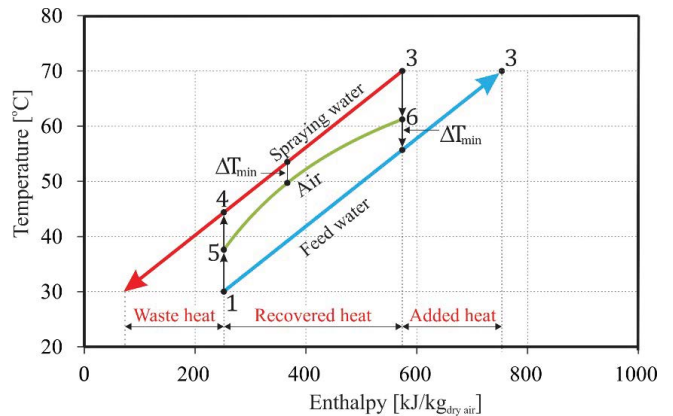


Fig. 3. Pinch analysis at $t_3 = 70^\circ\text{C}$, $t_1 = 30^\circ\text{C}$, $m = 3$ and $\Delta T_{min} = 5^\circ\text{C}$.

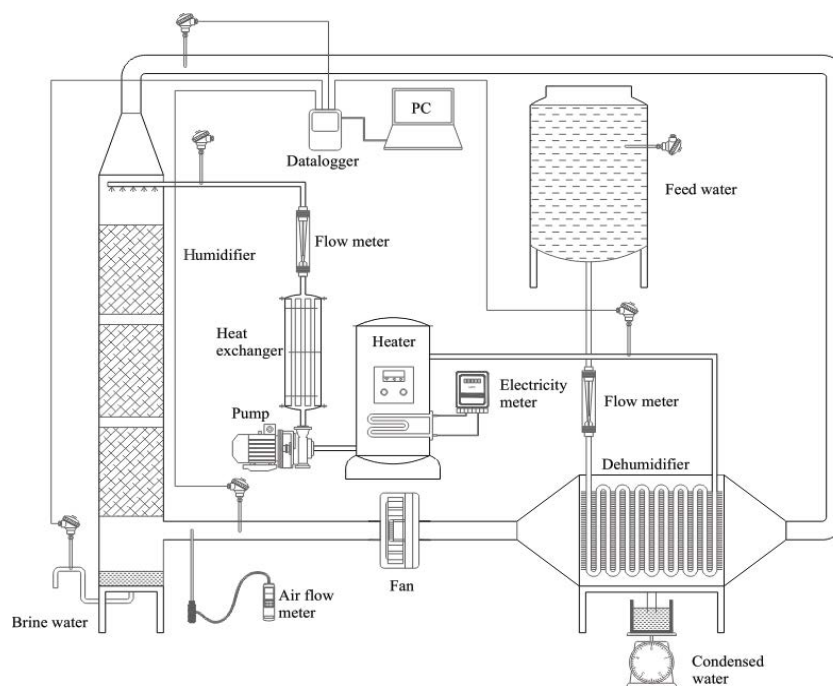


Fig. 4. Experimental model.

the water. Outside, the humidifier is covered by a layer of insulation material with a thickness of 2 cm. A copper fin tube coil is used for condensing water vapor in the dehumidifier. The total heat exchange area is 16 m². The dimensions of the dehumidifier are 23 cm height, 60 cm length and 55 cm width.

In the experimental process, the operating parameters of the system were measured in order to verify the theoretical results such as the mass flow rate and temperature of working fluids at the inlet and outlet of the humidifier and the dehumidifier, the temperature of hot water in the heater tank, the relative humidity of air at the inlet and outlet of humidifier and the productivity of the system. To measure flow rate of feed water and hot water; two flowmeters were used, with a range of 0.02–15 LPM and with an accuracy of $\pm 4\%$. These flow meters have been experimentally calibrated by comparing the displayed value of the flowmeter with the volume of water collected over a period of time. The first flowmeter was installed on the feed water pipe to measure the flow rate of feed water before entering the dehumidifier and the second one was installed on the hot water pipe to measure the flow rate of spraying water before entering the humidifier. Sea water used in the experimental model had a salinity of 26/1,000. To measure air flow, an anemometer (Testo 425) with a scale of 1–12 m/s and an accuracy of $\pm 0.1\%$ was used. Two humidity dataloggers (Testo 175H1) with an accuracy of $\pm 2\%$ and a resolution of 0.1% were used to measure the relative humidity of air. Temperature dataloggers (Testo 176T4) with an accuracy of $\pm 0.3^\circ\text{C}$ and resolution of 0.1°C were used to measure the temperatures of water and air at the inlet and outlet of the humidifier and dehumidifier. The hot water tank was heated by 2 resistors with a total capacity

of 18 kW. The fresh water productivity was measured by collecting the amount of condensed water in a glass cylinder.

4. Results and discussion

Based on Pinch technology, a simulation program has been developed. The flow chart of the theoretical simulation is shown in Fig. 5. To verify theoretical results, the experimental parameters were performed with the same theoretical parameters. The theoretical and experimental results are compared on the following graphs.

4.1. Effect of m on the temperature of water at the outlet of the humidifier and dehumidifier

The theoretical and experimental results in Fig. 6 show that, the temperature of feed water at the outlet of the dehumidifier (t_2) and the temperature of water at the outlet of the humidifier (t_4) varies with m and has the extreme point at the same value of m . At the extreme point, t_2 is maximized and t_4 is minimized. Because the mass flow rate of water in the humidifier equals to that of the dehumidifier, the heat recovered in the CAOW-HDD system is maximized when t_2 is maximized and t_4 is minimized. There is only one optimum value of m corresponding to the specific values of t_3 and t_1 .

4.2. Effect of m on the heat recovery ratio

The simulation and experimental results in Fig. 7 show that at the optimum value of m , heat recovery is maximized. At $t_3 = 80^\circ\text{C}$, $t_1 = 30^\circ\text{C}$ and $\Delta T_{\min} = 5^\circ\text{C}$, the optimum value of m and the heat recovery rate ratio are $m = 4$ and $f = 65\%$,

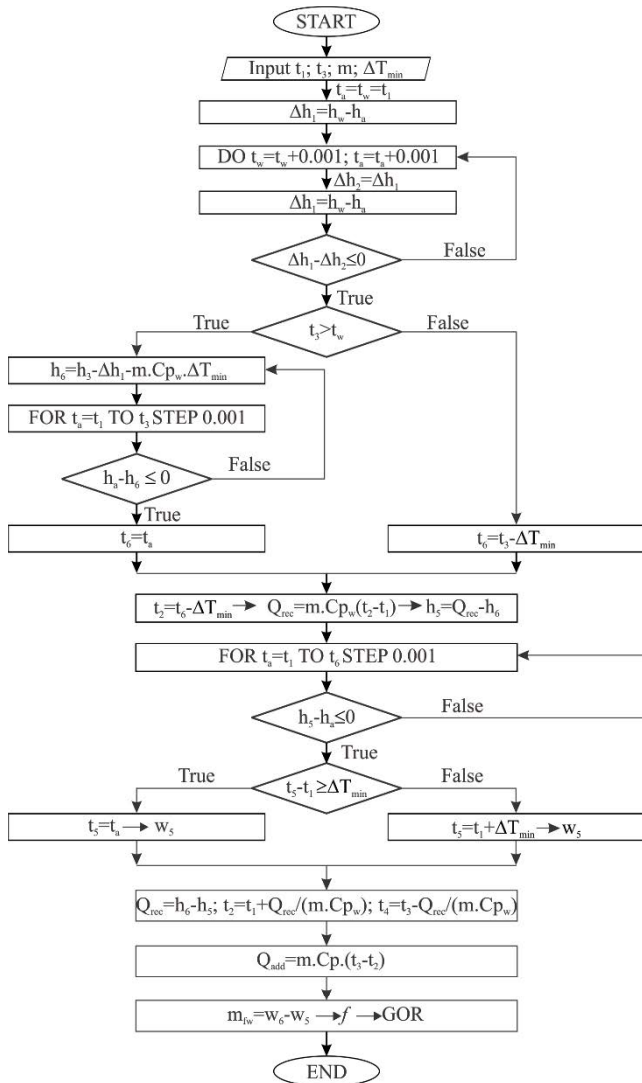


Fig. 5. Flow chart of theoretical modelling.

respectively. Compared to Hou et al. previous research results [7] under the same working conditions, the optimum value of m is the same ($m = 4$). This result shows that the simulation results are reliable.

4.3. Effect of m on the GOR

The simulation and experimental results in Fig. 8 confirm that GOR also depends on m . GOR is the ratio between the latent heat of condensation of water vapor in the air and the additional heat. When the heat recovery rate is at the maximum, the heat input is the smallest. Therefore, at the optimum value of m , the GOR is also maximized. At $t_3 = 70^\circ\text{C}$, $t_1 = 30^\circ\text{C}$ and $\Delta T_{\min} = 5^\circ\text{C}$, the optimum value of m and the heat recovery rate ratio are $m = 3$ and GOR = 1.6, respectively.

The simulation results in Fig. 9 indicate that the optimum value of m is independent to ΔT_{\min} . At the other values of ΔT_{\min} , the optimum GOR is obtained at the same value of m . The slope of the GOR curve is inversely proportional

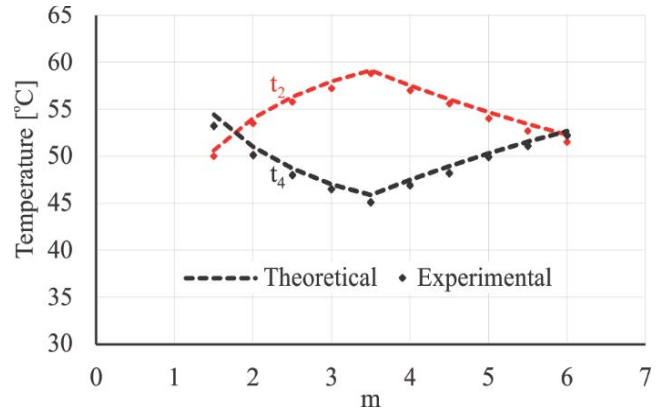


Fig. 6. Effect of m on t_2 at $t_1 = 30^\circ\text{C}$; $t_3 = 75^\circ\text{C}$; $\Delta T_{\min} = 5^\circ\text{C}$.

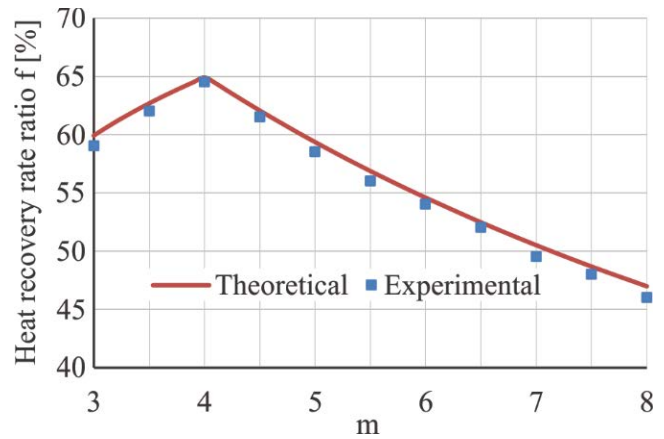


Fig. 7. Effect of m on the heat recovery ratio at $t_1 = 30^\circ\text{C}$; $t_3 = 80^\circ\text{C}$ and $\Delta T_{\min} = 5^\circ\text{C}$.

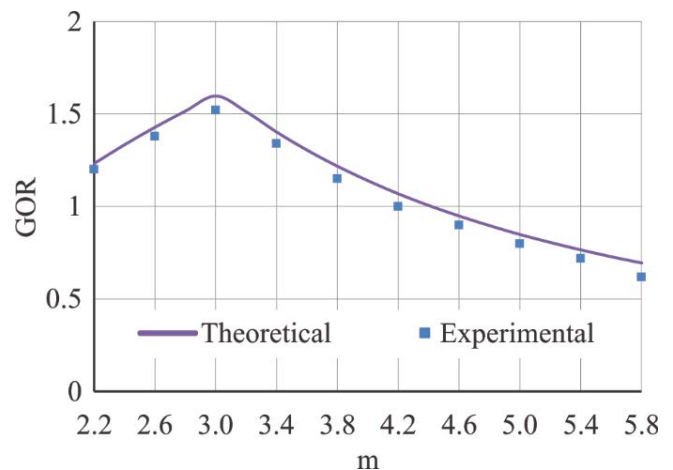


Fig. 8. Effect of m on the GOR at $t_3 = 70^\circ\text{C}$; $t_1 = 30^\circ\text{C}$ and $\Delta T_{\min} = 5^\circ\text{C}$.

to the ΔT_{\min} . At the optimum value of m , the GOR difference with ΔT_{\min} is the largest. The further away from the optimum value of m , the GOR difference with ΔT_{\min} is lower and tends to converge. At $t_3 = 70^\circ\text{C}$, $t_1 = 30^\circ\text{C}$ and $\Delta T_{\min} = 2^\circ\text{C}$ the optimum value of GOR is 2.68.

4.4. Effect of t_3 and ΔT_{min} on the optimum GOR

The simulation and experimental results in Fig. 10 show that, the lower ΔT_{min} , the higher the optimum GOR. At the lower value of ΔT_{min} , the higher the heat transfer efficiency

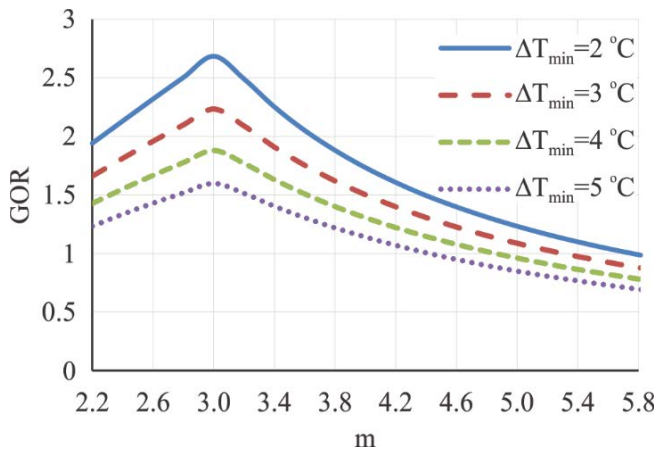


Fig. 9. Effect of m on the GOR at $t_3 = 70^\circ\text{C}$; $t_1 = 30^\circ\text{C}$.

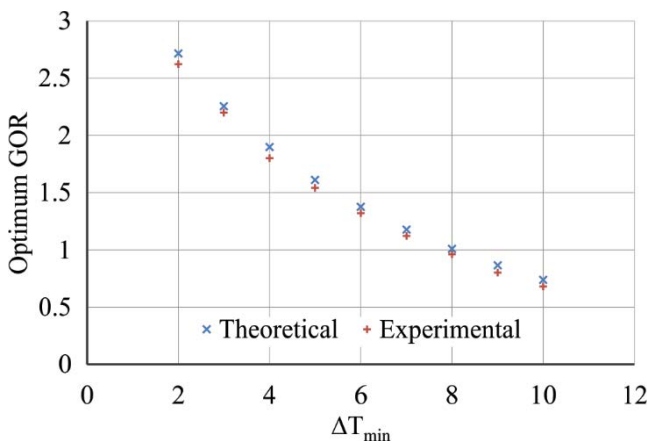


Fig. 10. Effect of ΔT_{min} on GOR at $t_3 = 70^\circ\text{C}$, $t_1 = 30^\circ\text{C}$.

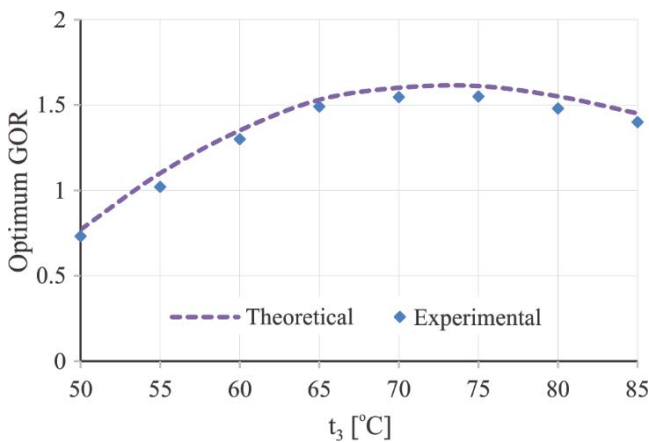


Fig. 11. Effect of t_3 on GOR at $\Delta T_{min} = 5^\circ\text{C}$ and $t_1 = 30^\circ\text{C}$.

and the more heat that is recovered, which increases the GOR. However, to achieve a low value of ΔT_{min} , the heat exchanger area must be larger.

The results in Fig. 11 confirmed that there is a range of temperatures for better optimum value of GOR corresponding to ΔT_{min} . In this temperature range, the optimum value of the GOR is the largest and there is almost no significant change. Outside this temperature range, the change in value of optimum GOR is significant.

The simulation results in Fig. 12 show that, the range of t_3 for the better optimum GOR varies with ΔT_{min} . At the same working parameters, the lower the ΔT_{min} , the higher the optimum GOR. At $\Delta T_{min} = 2$ °C, the maximum GOR reaches 2.86 corresponding to $t_3 = 60^\circ\text{C}$. At $\Delta T_{min} = 3$ °C, the maximum GOR reaches 2.29 corresponding to $t_3 = 66^\circ\text{C}$. At $\Delta T_{min} = 4$ °C, the maximum GOR reaches 1.9 corresponding to $t_3 = 69^\circ\text{C}$ – 70°C . At $\Delta T_{min} = 5$ °C, the maximum GOR reaches 1.62 corresponding to $t_3 = 71^\circ\text{C}$ – 74°C . The higher the ΔT_{min} , the higher the value of t_3 for the better optimum GOR.

According to Zheng [24], the suitable value of ΔT_{min} in the humidifier and dehumidifier is in the range of 3 °C–5 °C. Therefore, the t_3 in the CAOW-HDD system for the high GOR is in the range of 66 °C–74 °C.

4.5. Comparison with experimental results

As confirmed in the references [7,8,10–12], our experimental results also prove that the air entering and the air leaving the dehumidifier are saturated. The experimental results and theoretical results at the spraying water temperature of 70 °C and 75 °C with 3 flow rates are $m = 2.5$, $m = 3$ and $m = 3.5$ and the same ΔT_{min} are presented in Table 1.

The study results in Table 1 show that there is a negligible difference between experimental and theoretical results. Experimental results are always slightly less than that of the theoretical simulation due to ignoring heat loss to the environment and ignoring the evaporation of water into the air at the humidifier in the whole calculation process. The comparison between the theoretical and experimental temperatures are presented in Fig. 13.

The temperature measuring device used in the experimental model is the datalogger. When the system is operating stably, the data are recorded continuously for

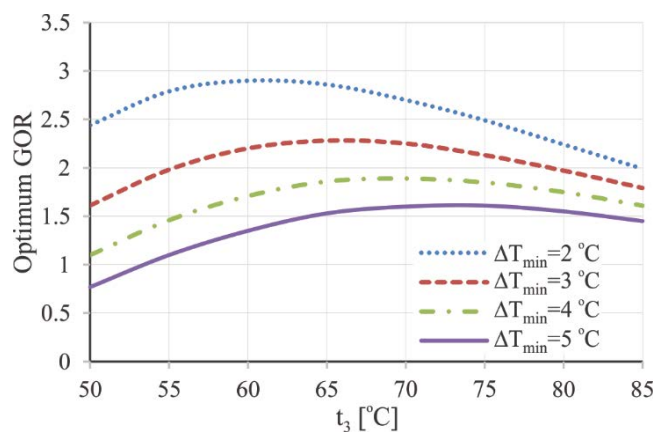


Fig. 12. Effect of t_3 and ΔT_{min} on GOR at $t_1 = 30^\circ\text{C}$.

Table 1
Experimental and theoretical results

t_3 (°C)	Experimental results					Theoretical results				
	m	t_2 (°C)	t_4 (°C)	t_5 (°C)	t_6 (°C)	m	t_2 (°C)	t_4 (°C)	t_5 (°C)	t_6 (°C)
70	2.5	54.7	41.9	39.6	59.5	2.5	55.0	43.3	40.0	60.1
70	3.0	54.8	43.3	38.0	61.2	3.0	55.1	43.9	38.5	61.5
70	3.5	53.5	44.0	37.4	62.5	3.5	53.9	44.8	38.3	62.9
75	2.5	56.9	42.3	40.3	61.4	2.5	58.1	44.1	41.7	62.1
75	3.0	58.2	44.8	38.8	62.9	3.0	58.4	45.6	39.1	63.2
75	3.5	55.9	45.4	38.5	63.9	3.5	56.3	46.8	39.2	64.5

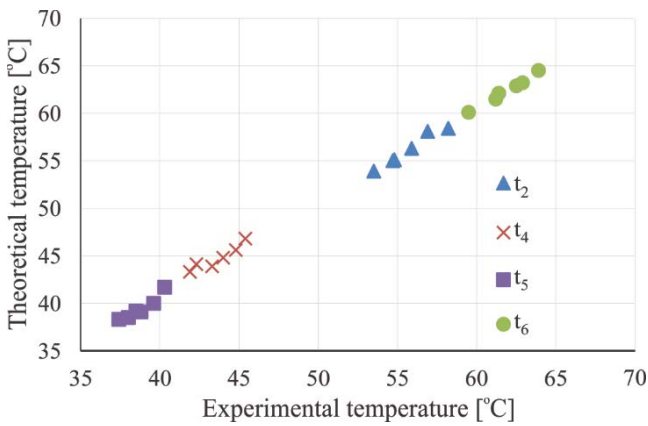


Fig. 13. Comparison between theoretical and experimental temperatures.

Table 2
Error analysis

Parameters	ϵ_{ar} (%)	ϵ_{max} (%)	ϵ_{min} (%)
t_2	0.84	2.1	0.34
t_4	2.63	4.14	1.52
t_5	0.82	1.04	0.64
t_6	1.84	3.6	0.77

5 min with a measurement step of 10s. The experimental value shown in Table 1 and the experimental error result shown in Table 2 are the average measured value over 5 min. Because the number of measurements is relatively large, the error of measuring equipment can be ignored in the calculation of experimental error. According to Zhani [25] the error of the experimental results can be evaluated by the following equation:

$$\epsilon = \frac{100}{k} \sum_{i=1}^k \frac{t_{exp(i)} - t_{sim(i)}}{t_{exp(i)}} \quad (9)$$

The error analysis results in Table 2 show that maximum relative error is 4.14% and minimum relative error is

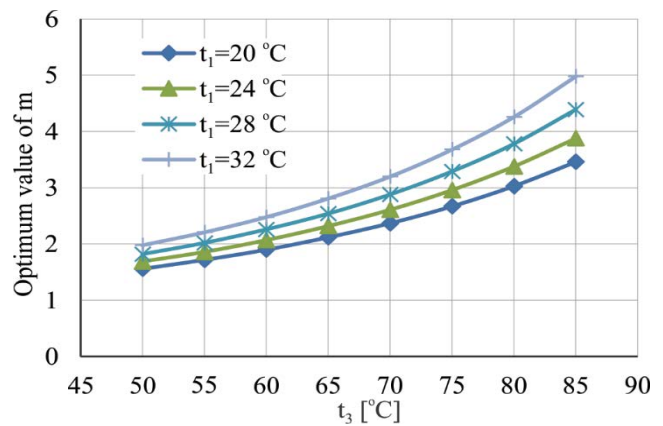


Fig. 14. Effect of t_3 and t_1 on the optimum value of m .

0.34%. The average error between theoretical and experimental results is around 2.63%. This shows the fit between experimental and the theoretical results.

4.6. Equation to determine the optimum value of m

The simulation results in Fig. 14 show that, the optimum value of m depends on t_3 and t_1 . The higher the temperature of spraying water and feed water, the higher the optimum value of m .

The mass flow rate of water and the mass flow rate of air in the humidifier and dehumidifier are equal. If the spraying water temperature (t_3) increases but m remains constant, it will cause the air temperature out of the humidifier (t_5) to increase and the air temperature out of the dehumidifier (t_6) to increase as well. The increase in air temperature leaving the dehumidifier reduces the heat recovered in the 1 dehumidifier. This air then passes through the humidifier and increases the temperature of the water leaving the humidifier (t_4). Similarly, when the feed water temperature (t_1) increases, but m remains constant, the amount of heat recovered in the dehumidifier will decrease and the temperature of the air leaving the dehumidifier will increase. Therefore, the higher the temperature of the spraying water and the feed water, the higher the optimum value of m .

The relationship between t_3 , t_1 and optimum value of m has been analyzed by IBM SPSS statistical software.

In which, the independent variable is t_3 and t_1 , and the dependent variable is the optimum value of m . The regression analysis results show that the correlation coefficient of t_3 is $R^2 = 1$ and correlation coefficient of t_1 is $R^2 = 0.998$. This result proves that these parameters are very closely related. The result of the analysis of variance also shows that $\text{Sig} = 0$. This result means that the regression model is perfectly suitable. From the regression analysis results, the equation to determine the optimum value of m in terms of t_3 and t_1 is given as Eq. (10).

$$m = A_1 + A_2 \cdot t_1 + A_3 \cdot t_1^2 + (A_4 + A_5 \cdot t_1 + A_6 \cdot t_1^2) \cdot t_3 + (A_7 + A_8 \cdot t_1 + A_9 \cdot t_1^2) \cdot t_3^2 \quad (10)$$

$A_1 = 2.17158$; $A_2 = -56.13066 \times 10^{-3}$; $A_3 = 40.87823 \times 10^{-4}$; $A_4 = -577.98932 \times 10^{-4}$; $A_5 = 25.9473 \times 10^{-4}$; $A_6 = -1.52178 \times 10^{-4}$; $A_7 = 769.1 \times 10^{-6}$; $A_8 = -2.6400 \times 10^{-6}$; $A_9 = 1.62732 \times 10^{-6}$.

Eq. (10) is applied in the temperature range/feed water $t_1 = 20^\circ\text{C}$ – 35°C with spraying water temperature $t_3 = 50^\circ\text{C}$ – 85°C and the same ΔT_{\min} .

5. Conclusions

From the theoretical and experimental studies on the CAOW-HDD system presented above, the following conclusions are drawn:

- By applying Pinch technology, a simulation program was built in order to do theoretical analysis on the CAOW-HDD system. The average errors between theoretical calculations and experimental data are less than 2.63% which confirm the faith in the presented theoretical method.
- The optimum value of m depends on the spraying water temperature t_3 , the feed water temperature t_1 and the minimum temperature difference (ΔT_{\min}). It is concluded that, at each optimum value of m , the heat recovery ratio f and the value of GOR are maximized as well. In order to gain the maximum value of GOR, it is shown that if the temperature t_3 is not high enough, the minimum temperature difference ΔT_{\min} should be decreased. In the case of $\Delta T_{\min} = 2^\circ\text{C}$, the GOR reaches the maximum value of 2.86 at $t_3 = 60^\circ\text{C}$.
- For each value of ΔT_{\min} , it is sure that there is an optimum value of t_3 for gaining the maximum value of GOR. Corresponding to the values of ΔT_{\min} ranging from 2°C – 5°C , the optimum values of t_3 vary from 60°C – 74°C .
- The mathematical equation used to determine the optimum value of m depending on the temperatures t_3 and t_1 was developed. By doing regression analysis, the correlation coefficients of t_3 and t_1 are $R^2 = 1$ and $R^2 = 0.998$, respectively.

Acknowledgement

We acknowledge the support of time and facilities from Ho Chi Minh City University of Technology (HCMUT), VNU-HCM, for this study.

Symbols

Cp	–	Heat capacity, $\text{kJ kg}^{-1} \text{K}^{-1}$
f	–	Heat recovery ratio, %
\dot{m}	–	Mass flow rate, kg s^{-1}
h	–	Enthalpy, kJ kg^{-1}
m	–	Mass flow rate ratio of water and air, –
Q	–	Thermal energy, kJ
r	–	Latent heat, kJ kg^{-1}
t	–	Temperature, $^\circ\text{C}$
Δt	–	Temperature difference, $^\circ\text{C}$
w	–	Humidity content, kg kg^{-1} dry air
e	–	Error

Subscripts

1, 2, 3, ...	–	Cycle points
a	–	Air
add	–	Add
exp	–	Experiment
min	–	Minimum
fw	–	Fresh water
sim	–	Simulation
rec	–	Recovery
w	–	Water
wa	–	Waste

Abbreviations

CAOW	–	Closed air open water
GOR	–	Gained output ratio
HDD	–	Humidification–dehumidification desalination

References

- [1] M. Al-Sahali, H.M. Ettouney, Humidification dehumidification desalination process: design and performance evaluation, *Chem. Eng. J.*, 143 (2008) 257–264.
- [2] A.E. Kabeel, M.H. Hamed, Z.M. Omara, S.W. Sharshir, Water desalination using a humidification–dehumidification technique—a detailed review, *Nat. Resour.*, 4 (2013) 286–305.
- [3] H. Muller-Holst, Solar Thermal Desalination Using the Multiple Effect Humidification (MEH)-Method Solar Desalination for the 21 Century, Vol. 18, L. Rizzuti, H. Ettouney, A. Cipollina, Eds., NATO Security Through Science Series: Springer, Netherlands, 2007, pp. 215–225.
- [4] G.P. Narayan, J.H. Lienhard V, Thermal design of humidification dehumidification systems for affordable small-scale desalination, *IDA J.*, 4 (2012) 24–34.
- [5] K.H. Mistry, A. Mitsos, J.H. Lienhard V, Optimal operating conditions and configurations for humidification–dehumidification desalination cycles, *Int. J. Therm. Sci.*, 50 (2011) 779–789.
- [6] K. Srithar, T. Rajaseenivasan, Recent fresh water augmentation techniques in solar still and HDH desalination – a review, *Renewable Sustainable Energy Rev.*, 82 (2018) 629–644.
- [7] S. Hou, S. Ye, H. Zhang, Performance optimization of solar humidification–dehumidification desalination process using Pinch technology, *Desalination*, 183 (2005) 143–149.
- [8] G. Prakash Narayan, M.H. Sharqawy, E.K. Summers, J.H. Lienhard V, S.M. Zubair, M.A. Antar, The potential of solar-driven humidification–dehumidification desalination for small-scale decentralized water production, *Renewable Sustainable Energy Rev.*, 14 (2010) 1187–1201.

- [9] M. Zamen, S.M. Soufari, S. Abbasian Vahdat, M. Amidpour, M.A. Zeinali, H. Izanloo, H. Aghababaie, Experimental investigation of a two-stage solar humidification–dehumidification desalination process, *Desalination*, 332 (2014) 1–6.
- [10] T.E. Simos, N.K. Nawayseh, M.M. Farid, A.A. Omar, S.M. Al-Hallaj, A.I. Tamimi, A simulation study to improve the performance of a solar humidification–dehumidification desalination unit constructed in Jordan, *Desalination*, 109 (1997) 277–284.
- [11] M.M. Farid, S. Parekh, J.R. Selman, S. Al-Hallaj, Solar desalination with a humidification–dehumidification cycle: mathematical modeling of the unit, *Desalination*, 151 (2003) 153–164.
- [12] J. Orfi, M. Laplante, H. Marmouch, N. Galanis, B. Benhamou, S.B. Nasrallah, C.T. Nguyen, Experimental and theoretical study of a humidification–dehumidification water desalination system using solar energy, *Desalination*, 168 (2004) 151–159.
- [13] G. Prakash Narayan, M.G. St. John, S.M. Zubair, J.H. Lienhard V, Thermal design of the humidification dehumidification desalination system: an experimental investigation, *Int. J. Heat Mass Transfer*, 58 (2013) 740–748.
- [14] M.H. Sharqawy, M.A. Antar, S.M. Zubair, A.M. Elbashir, Optimum thermal design of humidification dehumidification desalination systems, *Desalination*, 349 (2014) 10–21.
- [15] S.M. Soufari, M. Zamen, M. Amidpour, Performance optimization of the humidification–dehumidification desalination process using mathematical programming, *Desalination*, 237 (2009) 305–317.
- [16] X. Huang, T. Ke, Y. Li, X. Ling, Experimental investigation and optimization of total energy consumption in humidification–dehumidification system, *Energy Procedia*, 158 (2019) 3488–3493.
- [17] X. Huang, X. Ling, Y. Li, W. Liu, T. Ke, A graphical method for the determination of optimum operating parameters in a humidification–dehumidification desalination system, *Desalination*, 455 (2019) 19–33.
- [18] A.S.A. Mohamed, M.S. Ahmed, A.G. Shahdy, Theoretical and experimental study of a seawater desalination system based on humidification–dehumidification technique, *Renewable Energy*, 152 (2020) 823–834.
- [19] A.S.A. Mohamed, A.G. Shahdy, M. Salem Ahmed, Investigation on solar humidification dehumidification water desalination system using a closed-air cycle, *Appl. Therm. Eng.*, 188 (2021) 116621, doi: 10.1016/j.applthermaleng.2021.116621.
- [20] M. Alrbai, J. Enizat, H. Hayajneh, B. Qawasmeh, S. Al-Dahidi, Energy and exergy analysis of a novel humidification–dehumidification desalination system with fogging technique, *Desalination*, 522 (2022) 115421, doi: 10.1016/j.desal.2021.115421.
- [21] K.Q. Vo., A.Q. Hoang, C.H. Le, Optimizing the Operating Parameters of the Humidification–Dehumidification Desalination System by Pinch Technology, Presented at the 4th International Conference on Green Technology and Sustainable Development (GTSD), Ho Chi Minh City – Vietnam, 2018.
- [22] L. March, Introduction to Pinch Technology, Targeting House, Gadbroom Park, Northwich, Cheshire, CW9 7UZ, England, 1998.
- [23] ASHRAE Handbook—Fundamentals Volume (ASHRAE 1791 Tullie Circle), Atlanta, Georgia, 2001.
- [24] H. Zheng, Chapter 6 – Humidification–Dehumidification Solar Desalination Systems, In: *Solar Energy Desalination Technology*, Amsterdam, Elsevier, 2017, pp. 447–535.
- [25] K. Zhani, Solar desalination based on multiple effect humidification process: thermal performance and experimental validation, *Renewable Sustainable Energy Rev.*, 24 (2013) 406–417.

Appendix: Experimental images



Fig. A1. Front side of the humidifier presented in Fig. 4



Fig. A2. Inside space of the humidifier presented in Fig. 4.



Fig. A3. Checking the salinity of seawater.